ESC European Society of Cardiology

Cardiovascular Research (2022) **118**, 156–168
doi:10.1093/cvr/cvab041

Deficiency of inactive rhomboid protein 2 (iRhom2) attenuates diet-induced hyperlipidaemia and early atherogenesis

Carmen Hannemann [1,2,3], Johannes H. Schecker [1,2], Alica Brettschneider[1,2], Jana Grune[2,4], Nicole Rösener[1], Andrea Weller [1], Verena Stangl[1,2], Edward A. Fisher [3], Karl Stangl[1,2], Antje Ludwig[1,2,5†], and Bernd Hewing [1,2,6,7,8*†]

[1]Charité-Universitätsmedizin Berlin, corporate member of Freie Universität Berlin, Humboldt-Universität zu Berlin, Berlin Institute of Health, Medizinische Klinik für Kardiologie und Angiologie, Campus Mitte, Charitéplatz 1, 10117 Berlin, Germany; [2]DZHK (German Centre for Cardiovascular Research), partner site Berlin, Charitéplatz 1, 10117 Berlin, Germany, [3]Division of Cardiology, Department of Medicine, New York University School of Medicine, Hannemann435 East 30th St., 10016 New York, NY, USA; [4]Charité-Universitätsmedizin Berlin, corporate member of Freie Universität Berlin, Humboldt-Universität zu Berlin, Berlin Institute of Health, Institute of Physiology, Charitéplatz 1, 10117 Berlin, Germany; [5]Charité-Universitätsmedizin Berlin, corporate member of Freie Universität Berlin, Humboldt-Universität zu Berlin, Berlin Institute of Health, Klinik für Radiologie, Charitéplatz 1, 10117 Berlin, Germany; [6]Berlin Institute of Health (BIH), Anna-Louisa-Karsch-Straße 2, 10178 Berlin, Germany; [7]Zentrum für Kardiologie, Kardiologische Gemeinschaftspraxis, Loerstr. 19, 48143, Muenster, Germany; [8]Department of Cardiology III-Adult Congenital and Valvular Heart Disease, University Hospital Muenster, Albert-Schweitzer-Str. 33, 48149 Muenster, Germany

Received 19 May 2020; editorial decision 1 February 2021; accepted 9 February 2021; online publish-ahead-of-print 12 February 2021

Time for primary review: 18 days

Aims Atherosclerosis is a chronic inflammatory disease of the arterial vessel wall and anti-inflammatory treatment strategies are currently pursued to lower cardiovascular disease burden. Modulation of recently discovered inactive rhomboid protein 2 (iRhom2) attenuates shedding of tumour necrosis factor-alpha (TNF-α) selectively from immune cells. The present study aims at investigating the impact of iRhom2 deficiency on the development of atherosclerosis.

Methods and results Low-density lipoprotein receptor (LDLR)-deficient mice with additional deficiency of iRhom2 ($LDLR^{-/-}iRhom2^{-/-}$) and control ($LDLR^{-/-}$) mice were fed a Western-type diet (WD) for 8 or 20 weeks to induce early or advanced atherosclerosis. Deficiency of iRhom2 resulted in a significant decrease in the size of early atherosclerotic plaques as determined in aortic root cross-sections. $LDLR^{-/-}iRhom2^{-/-}$ mice exhibited significantly lower serum levels of TNF-α and lower circulating and hepatic levels of cholesterol and triglycerides compared to $LDLR^{-/-}$ mice at 8 weeks of WD. Analyses of hepatic bile acid concentration and gene expression at 8 weeks of WD revealed that iRhom2 deficiency prevented WD-induced repression of hepatic bile acid synthesis in $LDLR^{-/-}$ mice. In contrast, at 20 weeks of WD, plaque size, plaque composition, and serum levels of TNF-α or cholesterol were not different between genotypes.

Conclusion Modulation of inflammation by iRhom2 deficiency attenuated diet-induced hyperlipidaemia and early atherogenesis in $LDLR^{-/-}$ mice. iRhom2 deficiency did not affect diet-induced plaque burden and composition in advanced atherosclerosis in $LDLR^{-/-}$ mice.

* Corresponding author. Tel: +49 30450513286, E-mail: hewing@kardiologie-muenster.de
† These authors share senior authorship.

Graphical Abstract

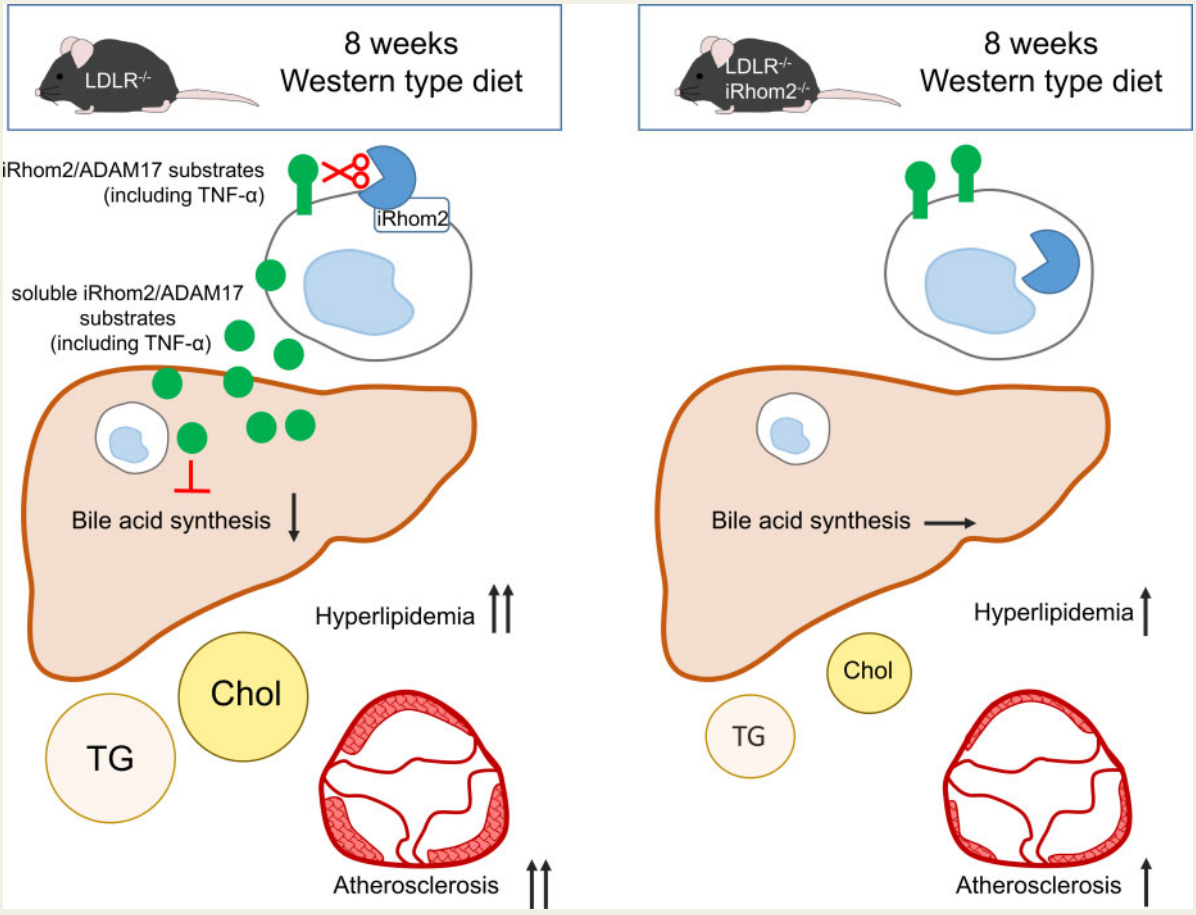

Keywords Atherosclerosis • iRhom2/Rhbdf2 • TNF-alpha • Inflammation

1. Introduction

Atherosclerosis is a chronic inflammatory disease of the arterial vessel wall and anti-inflammatory treatment strategies are currently pursued to lower cardiovascular disease burden.[1,2] The potent inflammatory cytokine TNF-α plays a substantial role in the pathogenesis of atherosclerosis.[3] Its contribution to atherosclerotic lesion development has been shown in various animal studies.[4–7] TNF-α is initially synthesized as a transmembrane protein and systemic release of soluble TNF-α requires ectodomain shedding mediated by *A Disintegrin And Metalloproteinase 17* (ADAM17, also known as TACE).[8] It has been discovered that maturation and activity of ADAM17 in haematopoietic cells is dependent on inactive rhomboid protein 2 (iRhom2).[9,10] Inhibition of iRhom2 prevents the secretion of ADAM17 substrates, most prominently TNF-α, selectively from immune cells without affecting the critical roles of ADAM17 substrates shed from non-immune cells in protection of skin and intestinal barrier function.[9–14] As iRhom2 deficiency allows a cell specific modulation of soluble TNF-α while preserving the function of transmembrane TNF-α, it offers potential advantages over a pan-TNF-α blockade by preventing the adverse side effects associated with the general inhibition of TNF-α signalling.[15,16] In mouse models of rheumatoid arthritis and lupus nephritis, it was shown that iRhom2 deficiency attenuates disease progression.[11,17] Besides shedding of TNF-α, iRhom2/ADAM17-mediated proteolytic release of inflammatory mediators such as chemokines, adhesion molecules, growth factors, and their receptors suggest a key role for iRhom2 in the pathogenesis of atherosclerosis.[18,19] This was supported by a recent study showing that siRNA knockdown of iRhom2 reduces the inflammatory and oxidative stress response of macrophage foam cells *in vitro*.[20] Until now, the effect of iRhom2 deficiency on the development of atherosclerosis has not been investigated. Hence, the present study aimed at

elucidating the impact of iRhom2 deficiency on the development of early and advanced atherosclerosis in LDLR-deficient mice after feeding a Western-type diet (WD) for 8 or 20 weeks.

2. Methods

2.1 Reagents

Unless otherwise specified, all reagents were purchased from Merck (Darmstadt, Germany).

2.2 Animals and diet

Animal experiments were approved under G0210/14 by the local authority (Landesamt für Gesundheit und Soziales, Berlin, Germany) and performed according to institutional guidelines, which conform to the guidelines from Directive 2010/63/EU of the European Parliament on the protection of animals used for scientific purposes. Low-density lipoprotein receptor-deficient ($LDLR^{-/-}$) mice (B6.129S7-*Ldlr*^{tm1Her}/J; JAX Mice, Boston, USA) and iRhom2-deficient ($iRhom2^{-/-}$) mice (kindly provided by Philipp Lang, Department of Molecular Medicine II, Universitätsklinikum Düsseldorf, Germany) were crossed to generate double heterozygous mice. Both, $LDLR^{-/-}$ and $iRhom2^{-/-}$ mice were originally backcrossed at least nine times to C57BL/6 mice. The resulting F1 generation was crossed to generate mice homozygous for $LDLR^{-/-}$ or homozygous for LDLR deficiency and iRhom2 deficiency ($LDLR^{-/-}iRhom2^{-/-}$). Genotypes were verified using polymerase chain reaction (PCR) and specific primers for iRhom2 and LDLR (Supplementary material online, *Table S1*). All mice were housed under specific-pathogen-free conditions and in a 12 h dark/12 h light cycle with access to food and water *ad libitum* at all times. Male $LDLR^{-/-}$ and $LDLR^{-/-}iRhom2^{-/-}$ mice were fed a Western-type diet (WD) containing 21.2% butter fat and 0.3% cholesterol (TD88137 mod., ssniff, Soest, Germany) for 8 or 20 weeks, starting from 10 weeks of age. Age-matched mice of both genotypes fed a low-fat control chow diet (CD) served as additional controls. All mice were randomly assigned to the different feeding conditions and were kept on CD before the start of the atherosclerosis study. General condition and body weight were monitored weekly. If indicated, food was weighed weekly to determine individual food intake. At the end of the diet, mice were anaesthetized and euthanized using the isoflurane drop jar method (containing 2–3 mL isoflurane, Forane®, Abbott Laboratories, Abbott Park, Illinois, USA, 1 mL isoflurane was re-loaded for each following mouse and adequate level of anaesthesia was confirmed by loss of pedal reflex) followed by terminal cardiac blood withdraw. After perfusion with phosphate-buffered saline (PBS) containing 10% sucrose, liver, heart, and aorta were dissected under a stereomicroscope. Pieces of liver and heart (containing the aortic root) were embedded in Tissue-Tek® O.C.T.™ compound (Sakura Finetek, Alphen aan den Rijn, The Netherlands), frozen on dry ice, and stored at -80°C. The aorta was fixed in 4% formalin (Roti®Histofix, Carl Roth, Karlsruhe, Germany) for 24 h at 4°C and stored in PBS at 4°C until further use. Additional pieces of the liver were shock-frozen in liquid nitrogen and stored at -80°C.

2.3 Analysis of serum lipids and cytokines

Whole blood was allowed to clot for at least 30 min at room temperature (RT) after collection. Serum was separated by centrifugation (8000 *g*, 10 min, RT) and stored at -80°C or at 4°C for lipid analysis. Total cholesterol (TC) and triglyceride (TG) concentrations were measured using enzymatic colorimetric assays (CHOL-PAP and TG GPO-PAP, Analyticon, Lichtenfels, Germany). The concentration of high-density lipoprotein cholesterol (HDL-C) was measured in supernatants following phosphotungstate-magnesium precipitation. Briefly, 40 µL of serum were mixed with 4 µL sodium phosphotungstate solution (40 g of phosphotungstic acid per litre in 160 mM NaOH) and 1 µL 2 M $MgCl_2$ and centrifuged (8000 *g*, 10 min, 4°C) for separation. Inflammatory cytokines and colony-stimulating factor 1 (CSF-1) were measured using multi-or singleplex bead-based assays (LEGENDplex™ Mouse Inflammation Panel; LEGENDplex™ Mouse HSC panel, M-CSF capture beads only, Biolegend, San Diego, USA) according to manufacturer's instructions. Serum samples were cleared from lipids by centrifugation (30 000 *g*, 15 min, 15°C) before incubation with beads.

2.4 Analysis of hepatic lipid and bile acid concentration

Approximately 30 mg of frozen liver was homogenized in 200 µL RIPA buffer (50 mM Tris–HCl pH 8.0, 150 mM NaCl, 1% Igepal® CA-630, 0.5% Sodium deoxycholate, 0.1% SDS) on ice. Cell debris was removed by centrifugation (8000 *g*, 1 min, RT) and the supernatant was assayed for TC and TG using enzymatic colorimetric assays (CHOL-PAP and TG GPO-PAP, Analyticon). Hepatic lipid content was normalized to protein concentration of the supernatants determined by Pierce® BCA Protein Assay (Thermo Fisher Scientific, Waltham, Massachusetts, USA). Bile acid concentration was measured using a Mouse Total Bile Acids Assay Kit (Crystal Chem, Zaandam, The Netherlands). Thawed liver tissue (60–80 mg) was homogenized in 1 mL 75% Ethanol in glass vials (Carl Roth), using a glass pestle. Hepatic bile acids were extracted at 50°C for 2 h and measured in supernatants after removing insoluble material (6000 x g, 10 min, 4°C). Hepatic bile acid concentration was normalized to liver weight.

2.5 Determination of lipoprotein lipase activity in adipose tissue

Lipoprotein lipase (LPL) activity was determined in adipose tissue (epididymal white adipose tissue) using a fluorometric kit (Cell Biolabs). Briefly, 200 mg of snap frozen adipose tissue was thawed, minced with scissors, and incubated at 37°C for 1 h in 600 µL 150 mM NaCl and 20 mM Tris pH 7.5 with 5 U/mL heparin (Biochrome) and 2 mg/mL fat free bovine serum albumin (Sigma). Samples were centrifuged (800 *g*, 15 min, 4°C) and supernatant was used in the LPL assay, which was performed according to the manufacturer's instructions. Fluorescence (485 nm excitation and 525 nm emission wavelengths) was detected with a GeminiEM plate fluorescence reader (Molecular Devices).

2.6 Liver histology and immunohistochemistry

Liver embedded in O.C.T. was cut in 6 µm sections using a cryostat (Leica, Wetzlar Germany). Per slide, three sections in a distance of 48 µm, were collected. Haematoxylin and eosin (H&E) staining was performed on acetone fixed sections using Harris modified haematoxylin solution and alcoholic Eosin Y solution. Formalin fixed sections were stained with filtered Oil Red O (ORO) solution to visualize lipids and counterstained with haematoxylin. Grading of steatohepatitis was performed according to previously described criteria[21,22] by an expert pathologist of iPATH.Berlin (Core Unit Immunopathology for Experimental Models of the Charité-Universitätsmedizin Berlin, Germany), blinded to the experimental conditions. To quantify hepatic neutrophil and macrophage content, acetone fixed slides were stained

with anti-mouse CD11b (clone M1/70, eBioscience™, Thermo Fisher Scientific, 1:200) after quenching autofluorescence with TrueBlack® (Biotium, Fremont, California, USA) following the manufacturer's instructions. For immunofluorescence, sections were stained with goat–anti rat Alexa Fluor® 488 (ab150165, Abcam, Cambridge, United Kingdom, 1:500) and mounted with VECTASHIELD with DAPI (Vector Laboratories, Burlingame, California, USA) to visualize cell nuclei. Sections stained without primary antibody served as negative controls (Supplementary material online, *Figure S1*). Approximately two to three fields per section (six to nine fields per animal) were imaged with BioRevo HS BZ 9000 (Keyence, Osaka, Japan) at the indicated magnifications and analysed using ImageJ software [National Institutes of Health (NIH), Bethesda, Maryland, USA] by a trained person blinded to the experimental conditions.

2.7 Staining and analysis of atherosclerotic lesions

Plaque distribution in the aorta was determined using the *en face* method. The adventitia was carefully dissected from the fixed aorta in PBS using a stereomicroscope. Following staining with ORO, aortas were placed in PBS, opened longitudinally, and pinned flat on a black surface on a silicone gel and the whole aorta or aortic arch region was photographed. Plaque area was analysed by a trained person blinded to the experimental conditions using ImageJ software and calculated as a percentage of ORO-positive area to total aortic arch area. The border of the aortic arch was defined from the junction of the myocardium to 2 mm distal from the left subclavian artery. The aortic root was cut in 6 µm sections using a cryostat (Leica). Plaque size was determined in ORO-stained sections (counterstained with haematoxylin) of 36 µm intervals in which all three aortic valve leaflets were present. Images were captured with BioRevo HS BZ 9000 (Keyence) and plaque size per aortic root was measured and calculated using ImageJ software by a trained person blinded to the experimental conditions.

Plaque macrophages were detected in aortic root cross-sections by immunohistochemistry using anti-CD68 (FA-11, Bio-Rad). Biotin-conjugated goat anti-rat IgG (Vector Laboratories) was used as secondary antibody. For detection of the biotinylated secondary antibody, the avidin/biotin complex (ABC)-alkaline phosphatase (AP) enzyme detection system in combination with the Vector Red Substrate was used and performed according to the manufacturer's instructions (Vector Laboratories). Negative controls (no primary antibody) were performed for all stainings. Plaque collagen content and necrotic core size was assessed in aortic root cross-sections by examination of Picro Sirius Red-stained arterial sections under polarizing light.

2.8 Quantitative real-time RT–PCR

RNA was isolated from 30 to 50 mg frozen liver tissue using Roti®Quick kit (Carl Roth) according to manufacturer's instructions. About 800 ng of total RNA was reversed-transcribed using the High-Capacity cDNA Reverse Transcription kit (Applied Biosystems, Thermo Fisher Scientific) according to manufacturer's instructions. TaqMan assays (Applied Biosystems, Thermo Fisher Scientific) were used to quantify the expression of selected mouse genes (Supplementary material online, *Table S2*) using the 7300 Real Time PCR System (Applied Biosystems, Thermo Fisher Scientific). Expression of target genes was calculated relative to the expression of a housekeeping gene (RPL19) using the comparative ΔCt method. Relative mRNA expression levels are presented as $2^{-\Delta\Delta Ct}$-values.

2.9 Flow cytometry

To analyse circulating monocyte subsets, whole blood collected in EDTA tubes was stained with anti-mouse CD45-APC (30-F11), CD115-PE (AFS98), and Ly6G/Ly6C-PB (RB6-8C5) antibodies. Erythrocytes were lysed with EasyLyse (Dako, Agilent, Santa Clara, California, USA) and samples were analysed with CyAn ADP Analyzer and Summit 4.4 software (Beckman Coulter, Inc., Fullerton, California, USA). Monocytes were defined as CD45- and CD115 (CSF-1R)-positive cells (CD45+ CD115+). Monocyte subpopulations were discriminated according to the expression of high or low levels of Ly6G/Ly6C (CD45+CD115+Ly6C$^{high/low}$). Blood leukocytes were counted using a hemocytometer. To identify lymphocyte populations, RBC-lysed EDTA blood was stained with CD45-APC (30-F11), CD3-PerCP (145-2C11), CD4-PE-Cy7 (GK1.5), CD8-BV510 (53-6.7), B220-FITC (RA3-6B2), NKp46-APC (29A1.4), and Zombie NIR (to discriminate live/dead cells). Subsequently, cells were fixed, permeabilized, stained with IFN-γ-PE (XMG1.2) to detect intracellular IFN-γ levels and analysed on MACSQuant Analyzer 10 (Miltenyi Biotec, Bergisch Gladbach, Germany). All antibodies were purchased from Biolegend.

2.10 Statistical analysis

Data analysis was performed using Prism, software version 7 (GraphPad, San Diego, California, USA). All data are presented as individual values, mean ± SEM or median in box (from 25th to 75th percentile) and whiskers (from smallest to highest value) plots, unless otherwise specified. Outliers, identified using the ROUT method ($Q = 1\%$), were excluded. Comparison between two groups was made using either unpaired Student's *t*-test or Mann–Whitney *U* test, when D'Agostino and Pearson tests for normal distribution was rejected. Unpaired *t*-test with Welch's correction was applied if variances were not equal between groups, as judged by *F*-test. Comparisons between genotype and diet were made using two-way analysis of variance (ANOVA) followed by Sidak's multiple comparison test. A *P*-value <0.05 was considered statistically significant. Pearson's correlation coefficient was calculated for correlation analyses between variables.

3. Results

3.1 Impact of iRhom2 deficiency on early atherosclerotic lesion development

LDLR$^{-/-}$ and LDLR$^{-/-}$iRhom2$^{-/-}$ mice were fed a WD for 8 weeks (8WD) to assess the influence of iRhom2 deficiency on early atherosclerotic lesion development. Evaluation of atherosclerotic plaques in the aortic arch using the *en face* method showed similar plaque areas in both genotypes (*Figure 1A*). Atherosclerotic plaque size, determined in aortic root cross-sections, was significantly reduced by 48% in iRhom2-deficient mice compared to LDLR$^{-/-}$ mice (*Figure 1B*). The plaque composition in the aortic root, relative plaque (CD68+) macrophage and collagen content, did not differ between both genotypes (*Figure 1C and D*).

3.1.1 Impact of iRhom2 deficiency on serum levels of inflammatory cytokines and distribution of blood monocyte subsets in LDLR$^{-/-}$ mice

As shown in *Figure 2A*, the 8WD-induced increase in serum TNF-α levels in LDLR$^{-/-}$ mice was not observed in LDLR$^{-/-}$iRhom2$^{-/-}$ mice. Serum TNF-α levels were significantly lower in WD-fed iRhom2-

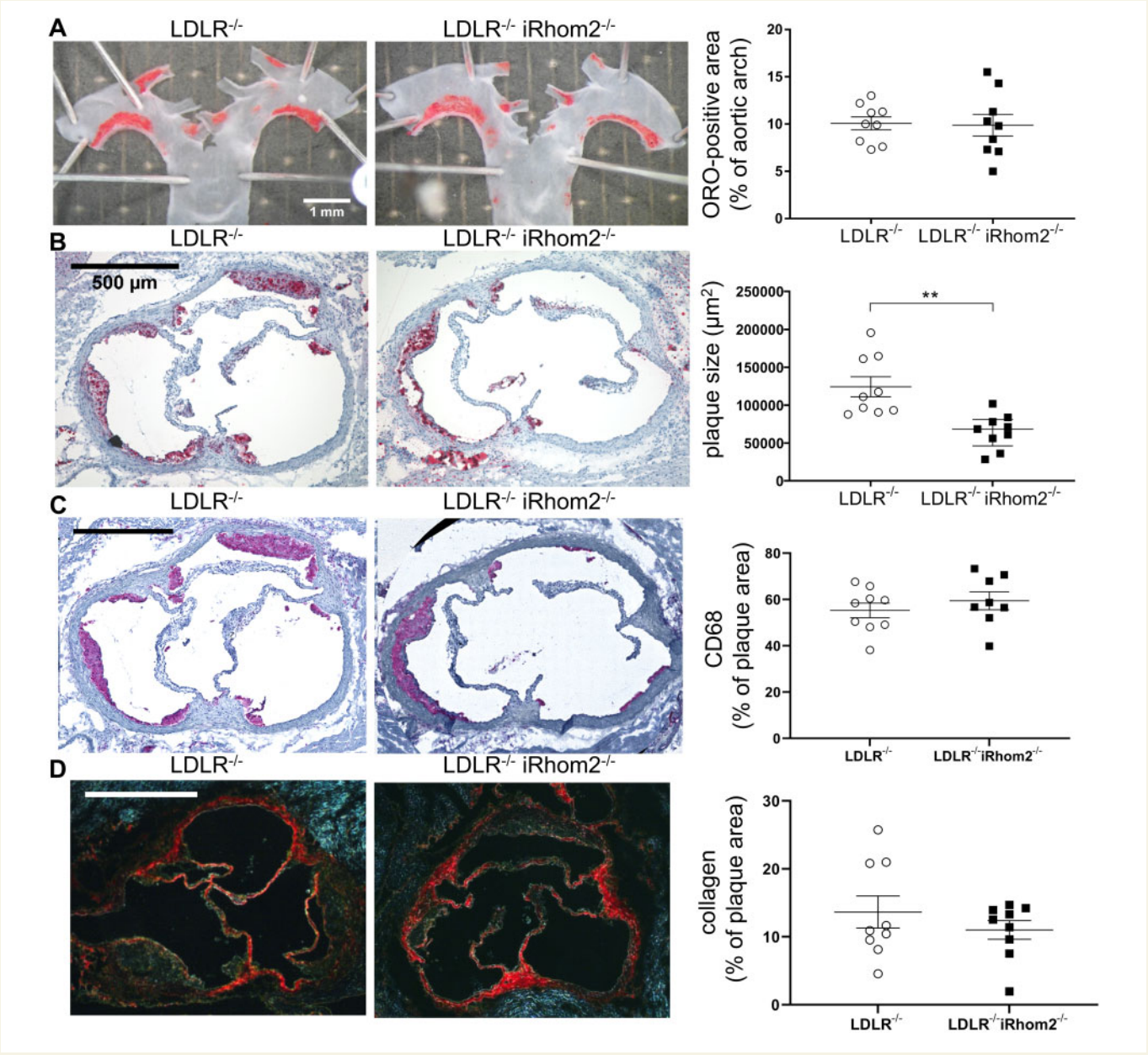

Figure 1 Inactive rhomboid protein 2 (iRhom2) deficiency attenuated early atherosclerotic plaque development in low-density lipoprotein receptor-deficient (LDLR$^{-/-}$) mice after feeding a Western-type diet (WD) for 8 weeks. (*A*) Representative images (left panel) and quantification (right panel) of *en face*, Oil Red O (ORO)-stained aortic arches. ORO-stained lipid area is displayed as percentage of total aortic arch area. Scale bar, 1 mm. (*B*) Representative images (left panel) and quantification of plaque size (right panel) of ORO-stained cross-sections of the aortic root. Scale bar, 500 µm. (*C*) Representative images (left panel) and quantification (right panel) of plaque macrophage content of CD68-stained aortic root cross-sections. (*D*) Representative images (left panel) and quantification (right panel) of plaque collagen content of Picro Sirius Red-stained aortic root cross-sections under polarized light. $n = 8–9$ mice per group. $^{**}P < 0.01$ vs. LDLR$^{-/-}$ mice by Student's *t*-test. Individual values and mean ± SEM are presented.

deficient LDLR$^{-/-}$ mice compared to WD-fed LDLR$^{-/-}$ mice. A moderate positive correlation ($r = 0.605$, $P = 0.0078$) between TNF-α levels and aortic root plaque size was observed (Supplementary material online, *Figure S2A*).

Serum levels of IFN-γ were higher in LDLR$^{-/-}$iRhom2$^{-/-}$ mice compared to LDLR$^{-/-}$ mice under CD and WD conditions. In WD-fed LDLR$^{-/-}$iRhom2$^{-/-}$ mice, serum IFN-γ levels were increased compared to CD-fed controls, whereas IFN-γ levels did not differ between CD- and WD-fed LDLR$^{-/-}$ mice (*Figure 2B*). We found no significant differences in serum levels of IL-1β, IL-6, IL-1α, IL-17A, IL-10, IFN-β, CCL2, GM-CSF, IL-23, or IL-27 between both genotypes (*Figure 2C* and *D*; Supplementary material online, *Figure S3*). *Figure 2E* shows that leukocyte counts were similar across all experimental groups. To identify the potential source of the increased IFN-γ levels observed in LDLR$^{-/-}$iRhom2$^{-/-}$ mice, we analysed the frequency of circulating B cells, T cells (CD4- and CD8-positive), NK cells and their intracellular IFN-γ expression. While we found no differences in frequencies of the analysed lymphocyte populations between both genotypes, the intracellular levels of IFN-γ

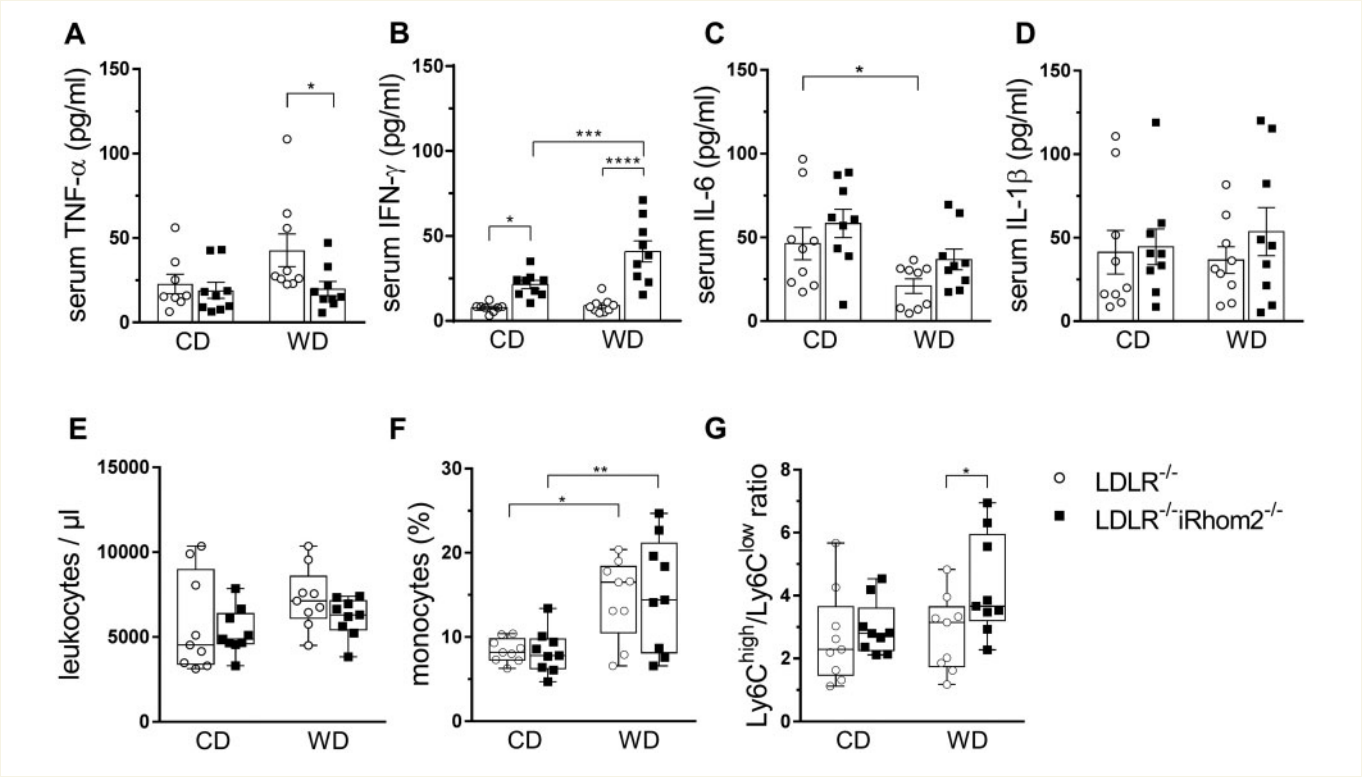

Figure 2 iRhom2 deficiency modulated serum levels of inflammatory cytokines and the ratio of Ly6C^{high} to Ly6C^{low} monocytes in LDLR$^{-/-}$ mice after feeding a Western-type diet for 8 weeks. Serum and EDTA-blood were collected from LDLR$^{-/-}$ and LDLR$^{-/-}$ iRhom2$^{-/-}$ mice fed a chow diet (CD) or Western-type diet (WD) for 8 weeks. Serum levels of (*A*) TNF-α, tumour necrosis factor α; (*B*) IFN-γ, interferon-γ; (*C*) interleukin (IL)-6 and (*D*) IL-1β were measured using bead-based immunoassays. Data are presented as individual values and mean ± SEM. (*E*) Leukocyte counts per µL EDTA-blood. (*F*) Percentage monocytes (CD115+) of total leukocytes (CD45+) and (*G*) ratio of Ly6C^{high} to Ly6C^{low} monocytes (CD45+CD115+Ly6C$^{high/low}$) determined by flow cytometry. $n = 8–9$ mice per group. Data are presented as individual values and median in box and whiskers plots. *$P < 0.05$, **$P < 0.01$, ***$P < 0.001$, ****$P < 0.0001$ vs. genotype or diet (as indicated) by two-way ANOVA followed by Sidak's multiple comparison test. LDLR, low-density lipoprotein receptor; iRhom2, inactive rhomboid protein 2; CD, chow diet; WD, Western-type diet.

were significantly higher in LDLR$^{-/-}$iRhom2$^{-/-}$ compared to LDLR$^{-/-}$ mice (Supplementary material online, *Figure S4*). Relative levels of circulating monocytes were increased in WD-compared to CD-fed mice, but did not differ between both genotypes (*Figure 2F*). Analysis of monocyte subsets revealed that WD-fed LDLR$^{-/-}$iRhom2$^{-/-}$ mice showed a trend towards higher levels of Ly6C^{high} and lower levels of Ly6C^{low} monocytes compared to LDLR$^{-/-}$ mice (Supplementary material online, *Figure S5A and B*). Overall, this resulted in a higher ratio of Ly6C^{high} to Ly6C^{low} monocytes in WD-fed LDLR$^{-/-}$iRhom2$^{-/-}$ mice in comparison to WD-fed LDLR$^{-/-}$ mice (*Figure 2G*). We determined serum levels of colony stimulating factor 1 (CSF-1) and expression of its receptor (CSF-1R) on circulating monocytes, both known substrates of ADAM17 and involved in promoting monocyte differentiation.[23–25] Expression of CSF-1R on circulating monocytes increased after feeding a WD, in particular on Ly6C^{high} monocytes (Supplementary material online, *Figure S5C–E*). There was a trend towards a higher CSF-1R expression on circulating Ly6C^{high} monocytes of LDLR$^{-/-}$iRhom2$^{-/-}$ compared to LDLR$^{-/-}$ mice (Supplementary material online, *Figure S5D*). Serum levels of the ligand, CSF-1, were similar between all experimental groups (Supplementary material online, *Figure S5F*).

3.1.2 Effect of iRhom2 deficiency on WD-induced hyperlipidaemia

Serum lipid levels were not affected by iRhom2 deficiency under CD conditions (*Figure 3A–C*). Eight weeks of WD-feeding severely increased serum lipid levels in both genotypes, but hyperlipidaemia was attenuated in iRhom2-deficient LDLR$^{-/-}$ mice as shown by reduced serum levels of TC and (non-fasting) TG compared to LDLR$^{-/-}$ mice (*Figure 3A and B*). Overall, LDLR$^{-/-}$iRhom2$^{-/-}$ mice displayed a lower atherogenic lipid profile compared to LDLR$^{-/-}$ mice, as represented by a lower TC/high-density lipoprotein cholesterol (HDL-C) ratio (*Figure 3C* and Supplementary material online, *Figure S6*). TC levels and aortic root plaque size showed a moderate positive correlation ($r = 0.515$, $P = 0.029$), (Supplementary material online, *Figure S2B*). As illustrated in *Figure 3D*, body weight was similar between both genotypes at the start and the end of WD. Weight progression on WD differed between LDLR$^{-/-}$iRhom2$^{-/-}$ mice compared to LDLR$^{-/-}$ mice with lower weight gain observed in iRhom2-deficient LDLR$^{-/-}$ mice during the first week of WD. The course of weight gain was verified in an independent set of mice and was not related to unequal food intake between both genotypes (*Figure 3E and F*).

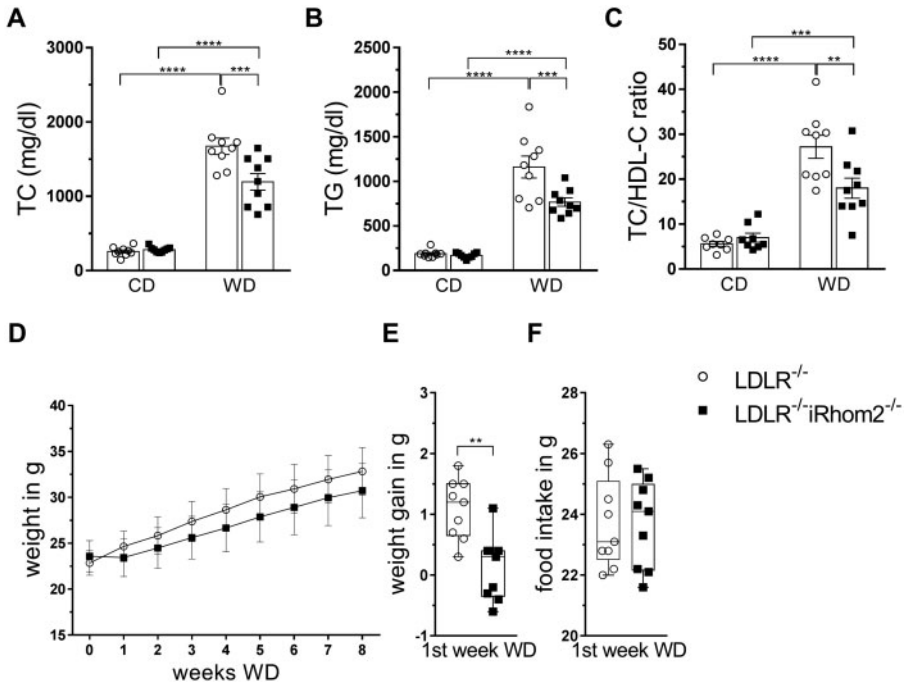

Figure 3 iRhom2-deficient LDLR$^{-/-}$ mice exhibited an attenuated hyperlipidaemia after 8 weeks of Western-type diet (WD). LDLR$^{-/-}$ and LDLR$^{-/-}$iRhom2$^{-/-}$ mice were fed a chow diet (CD) or WD for 8 weeks. Serum levels of TC, total cholesterol (*A*), TG, non-fasting triglycerides (*B*), and TC/HDL-C ratio, ratio of total cholesterol/high-density lipoprotein cholesterol (*C*) determined using enzymatic assays. Data are presented as individual values and mean ± SEM. (*D*) Weekly weight progression during WD. Data are presented as mean ± SD. $n = 8$–9 mice per group. $^{**}P < 0.01$, $^{***}P < 0.001$, $^{****}P < 0.0001$ vs. genotype or diet (as indicated) by two-way ANOVA followed by Sidak's multiple comparison test. (*E*) Individual weight gain and (*F*) food intake during the first week of WD. Data are presented as individual values and median in box and whiskers plots. $n = 9$ mice per group. $^{**}P<0.01$ vs. LDLR$^{-/-}$ mice by Student's *t*-test. LDLR, low-density lipoprotein receptor; iRhom2, inactive rhomboid protein 2.

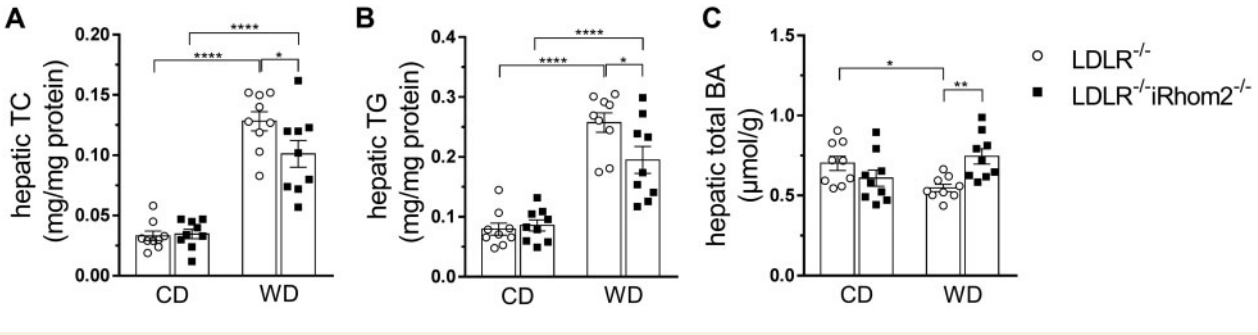

Figure 4 iRhom2 deficiency reduced Western-type diet (WD) induced hepatic lipid accumulation and maintained hepatic bile acid (BA) content in LDLR$^{-/-}$ mice after feeding a WD for 8 weeks. Livers of LDLR$^{-/-}$ and LDLR$^{-/-}$iRhom2$^{-/-}$ mice fed a chow diet (CD) or WD for 8 weeks were analysed for hepatic TC, total cholesterol (*A*), TG, triglycerides (*B*), and total bile acids (BA) (*C*) using enzymatic assays. Data are presented as individual values and mean ± SEM. $n = 9$ mice per group. $^{*}P < 0.05$, $^{**}P < 0.01$, $^{****}P < 0.0001$ vs. genotype or diet (as indicated) by two-way ANOVA followed by Sidak's multiple comparison test. LDLR, low-density lipoprotein receptor; iRhom2, inactive rhomboid protein 2.

3.1.3 Impact of iRhom2 deficiency on hepatic lipid accumulation and bile acid synthesis

After 8WD, LDLR$^{-/-}$ and LDLR$^{-/-}$iRhom2$^{-/-}$ mice showed a marked increase in hepatic TC and TG content. In comparison to WD-fed LDLR$^{-/-}$ mice, hepatic TC and TG levels were significantly lower in WD-fed iRhom2-deficient LDLR$^{-/-}$ mice (*Figure 4A and B*). In order to elucidate potential mechanisms by which iRhom2 deficiency attenuates WD-induced hyperlipidaemia and hepatic lipid accumulation, we measured

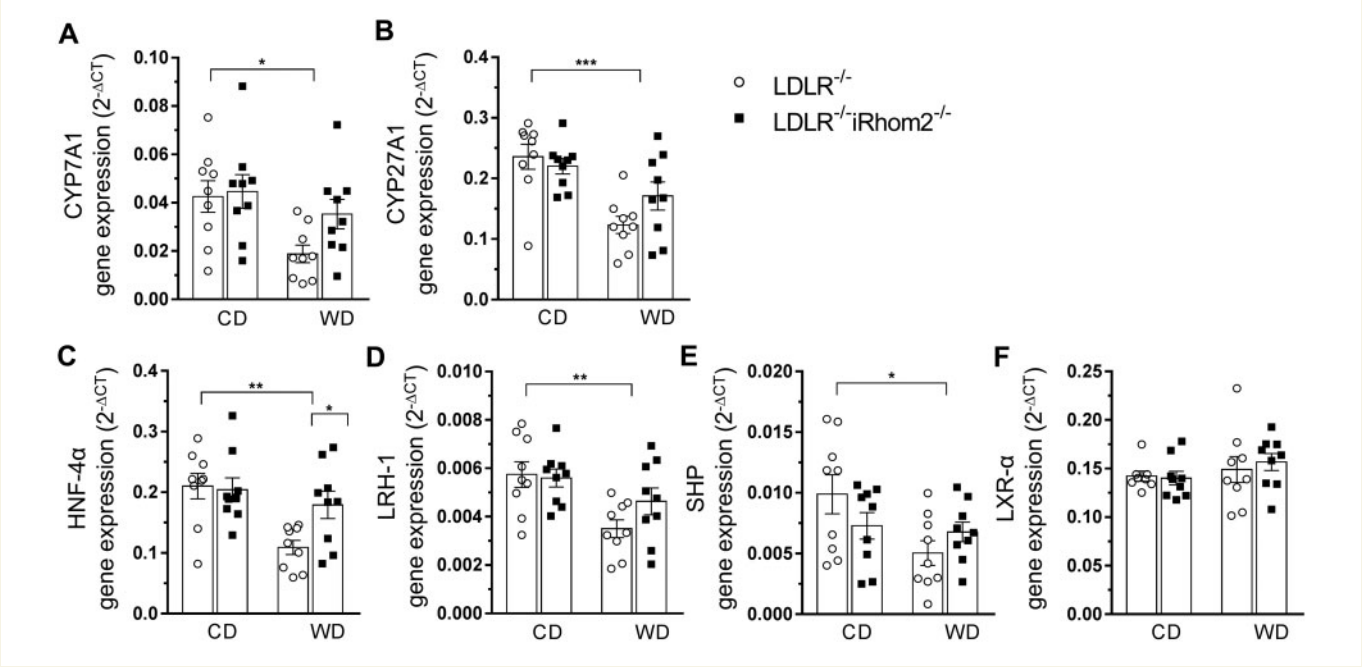

Figure 5 iRhom2 deficiency attenuated Western-type diet (WD)-induced suppression of genes involved in hepatic bile acid synthesis in LDLR$^{-/-}$mice after feeding a WD for 8 weeks. Gene expression was determined in livers of LDLR$^{-/-}$ and LDLR$^{-/-}$iRhom2$^{-/-}$ mice fed a chow diet (CD) or WD for 8 weeks by quantitative RT–PCR. (*A*) CYP7A1, cholesterol 7α-hydroxylase. (*B*) CYP27A1, sterol 27-hydroxylase. (*C*) HNF-4α, hepatocyte nuclear factor-4α. (*D*) LRH-1, liver receptor homolog 1. (*E*) SHP, small heterodimer partner. (*F*) LXR-α, liver x receptor-α. Data are presented as individual values and mean ± SEM. $n = 8$–9 mice per group. *$P < 0.05$, **$P < 0.01$, ***$P < 0.001$ vs. genotype or diet (as indicated) by two-way ANOVA followed by Sidak's multiple comparison test. LDLR, low-density lipoprotein receptor; iRhom2, inactive rhomboid protein 2.

the content of hepatic bile acids (BA), which represent the final transport form for the excretion of excess cholesterol from the body, as part of reverse cholesterol transport pathway.[26] Hepatic BA concentration was significantly decreased in WD-fed LDLR$^{-/-}$ mice compared to CD-fed controls (*Figure 4C*). In LDLR$^{-/-}$iRhom2$^{-/-}$ mice, hepatic BA content was not reduced by WD-feeding and was significantly higher compared to WD-fed LDLR$^{-/-}$ mice. Gene expression analyses revealed a differential expression of hepatic regulators of BA homeostasis between both genotypes: hepatic mRNA expression of cholesterol 7α-hydroxylase (CYP7A1) and sterol 27-hydroxylase (CYP27A1), key enzymes of the classic and alternative BA synthesis pathways,[27] was significantly repressed in WD-fed LDLR$^{-/-}$ mice as compared to CD-fed controls, while this down-regulation was attenuated in LDLR$^{-/-}$iRhom2$^{-/-}$ mice (*Figure 5A and B*). Furthermore, iRhom2 deficiency attenuated WD-induced down-regulation of transcriptional activators of CYP7A1, hepatocyte nuclear factor-4α (HNF-4α) and liver receptor homolog 1 (LRH-1),[28] that was observed in LDLR$^{-/-}$ mice (*Figure 5C and D*). Similarly, WD-feeding reduced mRNA expression of short heterodimer partner (SHP), an essential factor mediating BA-induced regulation of CYP7A1 expression[29] and triglyceride homeostasis[30] in LDLR$^{-/-}$ mice compared to CD-fed controls, whereas SHP expression remained unchanged in LDLR$^{-/-}$iRhom2$^{-/-}$ mice (*Figure 5E*). Gene expression of liver x receptor (LXR-α), which mediates cholesterol-induced up-regulation of CYP7A1 mRNA[31] (*Figure 5F*) and expression of other key regulators of hepatic cholesterol metabolism did not differ between LDLR$^{-/-}$ and LDLR$^{-/-}$iRhom2$^{-/-}$ mice (Supplementary material online, *Figure S7*). Activity of LPL, an enzyme which hydrolyses TG in very-LDL (VLDL) and chylomicrons, was determined in epididymal white adipose tissue and was not different between both genotypes (Supplementary material online, *Figure S8*).

3.1.4 Influence of iRhom2 deficiency on markers of hepatic inflammation

To examine whether a reduced hepatic immune cell infiltration is associated with the maintenance of BA synthesis and the resulting reduction of hyperlipidaemia in LDLR$^{-/-}$iRhom2$^{-/-}$ mice at 8WD, we quantified CD11b positive areas in the liver, which marks Kupffer cells and newly invaded monocytes/macrophages and neutrophils.[32] LDLR$^{-/-}$ and LDLR$^{-/-}$iRhom2$^{-/-}$ mice showed a strong WD-associated hepatic infiltration of CD11b-positive (CD11b+) cells, which was more pronounced in iRhom2-deficient LDLR$^{-/-}$ mice compared to LDLR$^{-/-}$ mice (*Figure 6A and B*). WD-induced hepatic gene expression of chemokine (CC motif) ligand 2 (CCL2), also known as macrophage chemoattractant protein, was similar between both genotypes (*Figure 6C*). Evaluation of hepatic histopathology showed that WD-fed mice displayed an aggravation of the grade of steatohepatitis compared to CD-fed mice, which was not different between WD-fed LDLR$^{-/-}$ and LDLR$^{-/-}$iRhom2$^{-/-}$ mice (*Figure 6A and D*).

3.2 Impact of iRhom2 deficiency on advanced atherosclerosis

After feeding a WD for 20 weeks, atherosclerosis area (whole aorta and aortic arch) as determined by the *en face* method, and aortic root plaque

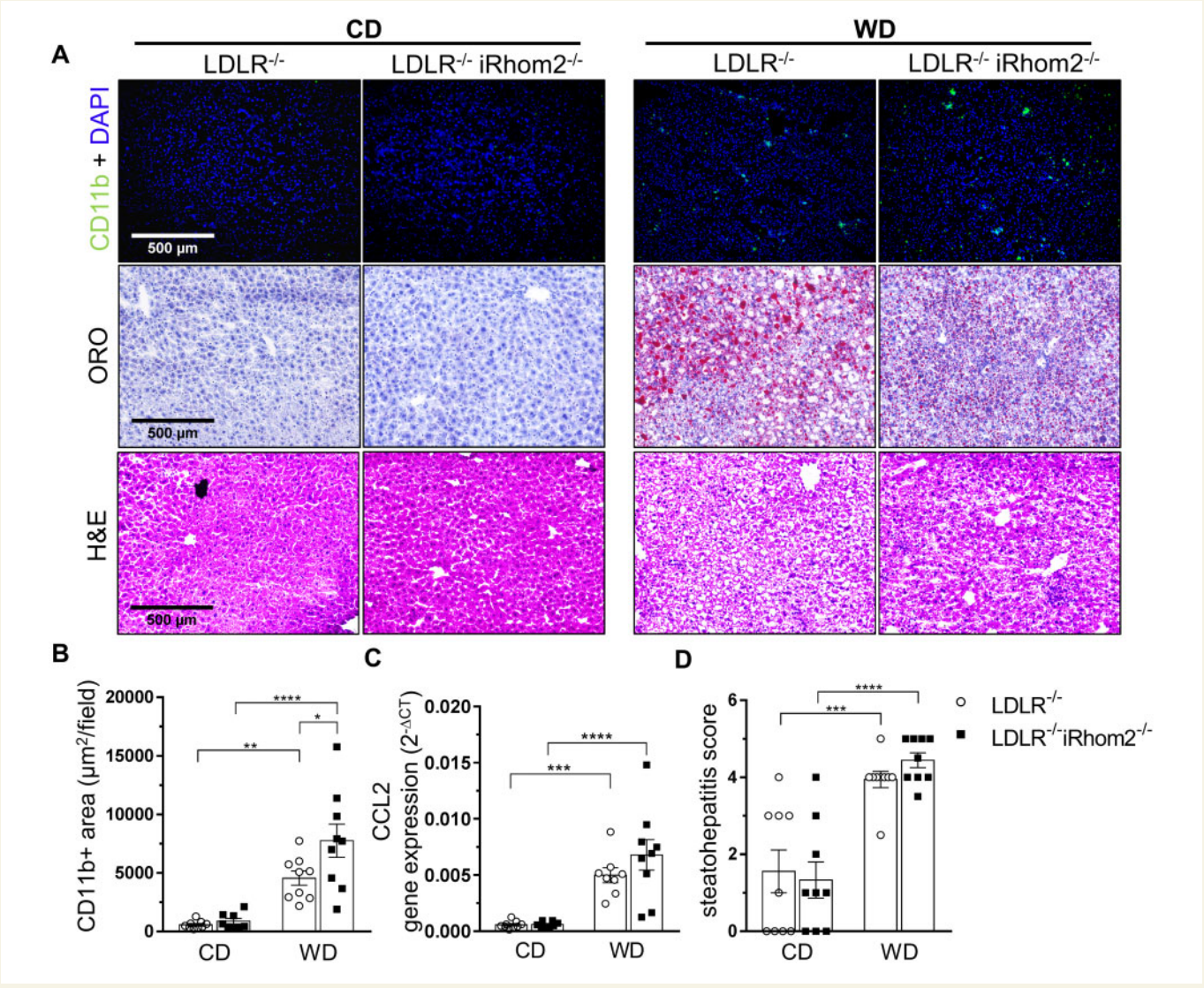

Figure 6 Markers of hepatic inflammation and histology of LDLR$^{-/-}$ and LDLR$^{-/-}$iRhom2$^{-/-}$ mice after feeding a Western-type (WD) diet for 8 weeks. LDLR$^{-/-}$ and LDLR$^{-/-}$iRhom2$^{-/-}$ mice were fed a chow diet (CD) or WD for 8 weeks. (*A*) Representative images of liver cryosections stained for CD11b and DAPI (4',6-diamidino-2-phenylindole) (upper panel), with ORO (Oil Red O) (middle panel) and H&E (haematoxylin and eosin) (lower panel). Scale bar, 500 µm. (*B*) Quantification of CD11b-positive (CD11b+) area per field. (*C*) Gene expression of CCL2 (chemokine CC motif ligand 2). (*D*) Grading of steatohepatitis. Data are presented as individual values and mean ± SEM. $n = 8$–9 mice per group. *$P < 0.05$, **$P < 0.01$, ***$P < 0.001$, ****$P < 0.0001$ vs. genotype or diet (as indicated) by two-way ANOVA followed by Sidak's multiple comparison test. LDLR, low-density lipoprotein receptor; iRhom2, inactive rhomboid protein 2.

size as measured in aortic root cross-sections did not differ between LDLR$^{-/-}$ and LDLR$^{-/-}$iRhom2$^{-/-}$mice (*Figure 7A* and Supplementary material online, *Figure S9*). We found no differences concerning relative plaque (CD68+) macrophage and collagen content, and necrotic core area in aortic root plaques between genotypes (*Figure 7B–D*). Circulating levels of TNF-α, IFN-γ, IL-6, and IL-1β were similar between both genotypes and diets (CD and WD) (*Figure 7E–H*). Diet-induced hypercholesteremia was not different between LDLR$^{-/-}$ and LDLR$^{-/-}$iRhom2$^{-/-}$ mice, whereas non-fasting triglyceride levels were attenuated by iRhom2 deficiency (*Figure 7I and J*). Hepatic mRNA expression of regulators of bile acid synthesis, CYP7A1 and HNF4α, was similar between both genotypes and diets (*Figure 7K and L*).

4. Discussion

The present study showed stage-specific effects of iRhom2 deficiency on atherogenesis in LDLR$^{-/-}$ mice. iRhom2 deficiency attenuated early atherogenesis in LDLR$^{-/-}$ mice by preventing diet-induced dysregulation of hepatic BA synthesis and attenuating hyperlipidaemia. In contrast, no beneficial effects of iRhom2 deficiency were observed in advanced stage atherosclerosis.

After 8 weeks of WD, we found a similar plaque deposition at atherosclerosis-prone sites in the aorta of LDLR$^{-/-}$ and LDLR$^{-/-}$iRhom2$^{-/-}$ mice, but a significantly smaller atherosclerotic lesion thickness in the aortic root of iRhom2-deficient LDLR$^{-/-}$ mice. This

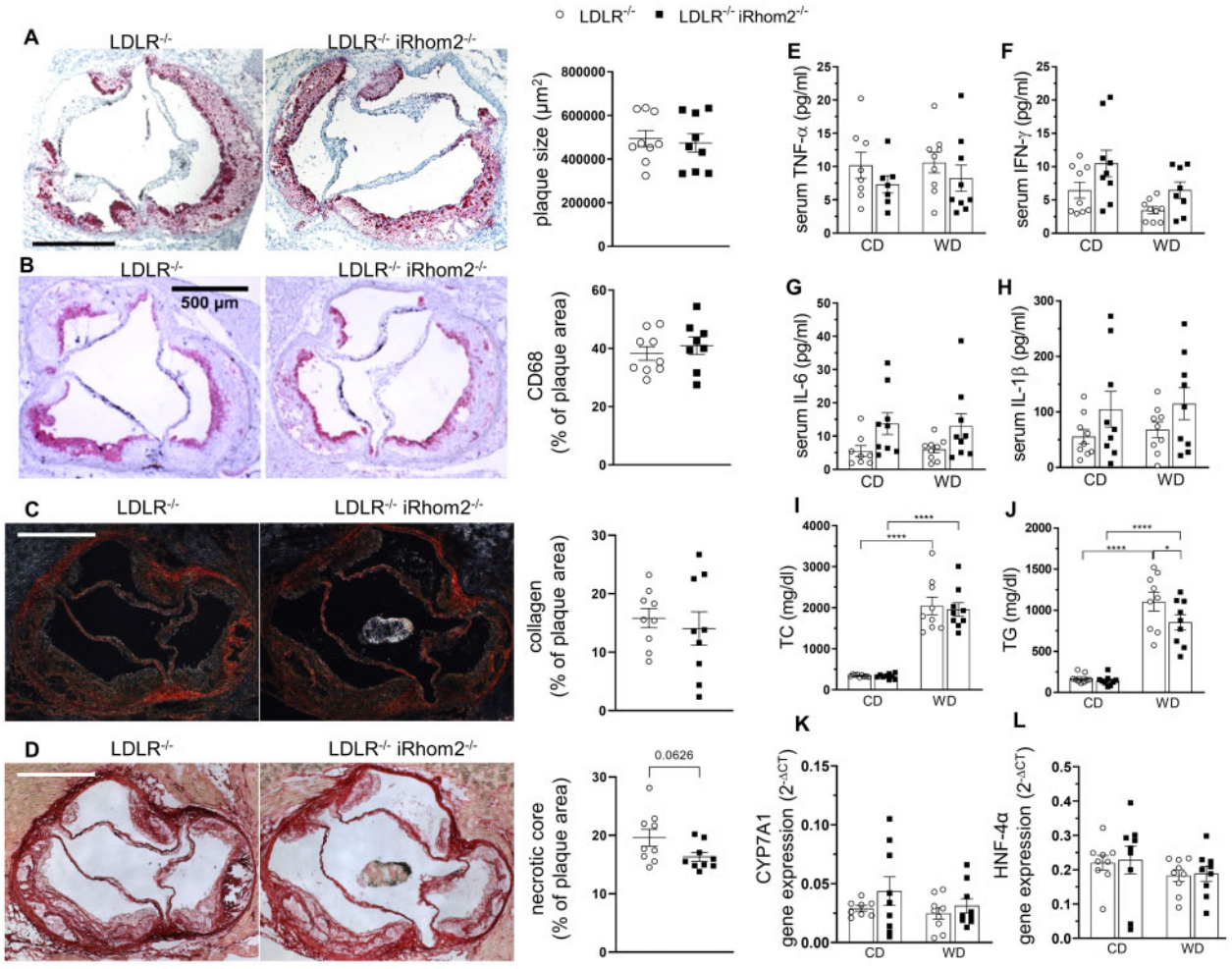

Figure 7 iRhom2 had no impact on advanced atherosclerosis in 20 weeks Western-type diet (WD)-fed low-density lipoprotein receptor-deficient ($LDLR^{-/-}$) mice. (*A*) Representative images (left panel) and quantification of plaque size (right panel) of ORO-stained cross-sections of aortic root. Scale bar, 500 µm. (*B*) Representative images (left panel) and quantification (right panel) of plaque macrophage content of CD68-stained aortic root cross-sections. (*C*) Representative images (left panel) and quantification (right panel) of plaque collagen content of Picro Sirius Red-stained aortic root cross-sections under polarized light. (*D*) Representative images (left panel) and quantification (right panel) of relative necrotic core area of Picro Sirius Red-stained aortic root cross-sections. $n = 8–9$ mice per group. $P = 0.0626$ vs. $LDLR^{-/-}$ mice by Student's *t*-test. Serum levels of (*E*) TNF-α, (*F*) IFN-γ, (*G*) IL-6, (*H*) IL-1β, (*I*) total cholesterol (TC), and (*J*) non-fasting triglycerides (TG) of 20 weeks WD-fed $LDLR^{-/-}$ and $LDLR^{-/-}iRhom2^{-/-}$ mice and age-matched chow diet (CD) fed mice. $^{*}P < 0.05$, $^{****}P < 0.0001$ vs. genotype or diet (as indicated) by two-way ANOVA followed by Sidak's multiple comparison test. Gene expression was determined in livers of 20 weeks WD-fed $LDLR^{-/-}$ and $LDLR^{-/-}iRhom2^{-/-}$ mice and age-matched chow diet (CD) fed mice by quantitative RT-PCR. (*K*) CYP7A1, cholesterol 7α-hydroxylase and (*L*) HNF-4α, hepatocyte nuclear factor-4α. $n = 7–9$ mice per group. All data are presented as individual values and mean ± SEM. LDLR, low-density lipoprotein receptor; iRhom2, inactive rhomboid protein 2.

indicates that iRhom2 deficiency may primarily attenuate processes that accelerate plaque growth rather than those that initiate plaque formation. We initially hypothesized that the lack of iRhom2 reduces WD-induced systemic inflammation in $LDLR^{-/-}$ mice and thus alleviates atherosclerosis. As anticipated, no increase in serum levels of TNF-α was detectable in 8 weeks WD-fed iRhom2-deficient $LDLR^{-/-}$ mice, resulting in significantly lower TNF-α levels compared to $LDLR^{-/-}$ mice; this may have contributed to the attenuation of early atherogenesis as supported by the correlation between circulating TNF-α levels and aortic root plaque size in our model. However, iRhom2 deficiency led to an increase in serum IFN-γ levels in CD- and WD-fed mice. In line with the previously described increased production of IFN-γ by human NK cells under ADAM17 inhibition,[33] our flow cytometry data indicate that NK cells may be a relevant source of the increased IFN-γ levels observed in $LDLR^{-/-}iRhom2^{-/-}$ mice at 8 weeks of WD. Furthermore, we found a shift in monocyte subpopulations in favour of $Ly6C^{high}$ monocytes in 8 weeks WD-fed $LDLR^{-/-}iRhom2^{-/-}$ mice. The conversion from $Ly6C^{high}$ into more mature $Ly6C^{low}$ monocytes is thought to be promoted by CSF-1R signalling.[23,34] CSF-1R and the cell surface form of CSF-1 are substrates of ADAM17 and shedding of their ectodomains from immune cells has been shown to be impaired by iRhom2 deficiency.[24,25,35,36] In accordance, we consistently found a trend towards higher expression of CSF-1R on monocytes in iRhom2-deficient $LDLR^{-/-}$ mice. Serum levels of CSF-1 did not differ between

genotypes, however, it is known that cell surface CSF-1 does not significantly contribute to circulating CSF-1 levels (which are predominantly formed by two secreted CSF-1 isoforms that are independent of ADAM17 shedding).[37] In addition to serum CSF-1, an enhanced autocrine signalling of cell surface CSF-1 may have contributed to the shift in monocyte subpopulations observed in iRhom2-deficient LDLR$^{-/-}$ mice.

Hence, iRhom2 deficiency affected certain markers of systemic inflammation associated with atherosclerosis,[38,39] but did not result in a clear atheroprotective pattern (lower levels of TNF-α, higher levels of IFN-γ, increased Ly6C$^{high/low}$ ratio) in our model. The most obvious atheroprotective effect of iRhom2 deficiency we detected was the attenuation of WD-induced hyperlipidaemia, a major trigger of atherosclerotic plaque development, after 8 weeks of WD-feeding. We found decreased TC levels, TC/HDL-C ratio, and reduced hepatic lipid accumulation in LDLR$^{-/-}$iRhom2$^{-/-}$ mice compared to LDLR$^{-/-}$ mice after 8 weeks of WD. It has been shown in cell culture and animal models that TNF-α is a negative regulator of hepatic BA synthesis and thereby leads to cholesterol accumulation.[40–43] We hypothesized that a more efficient BA synthesis and thus a potentially higher capacity to excrete excess cholesterol and lipids by bile secretion is the mechanism by which iRhom2 deficiency reduces hyperlipidaemia in 8 weeks WD-fed LDLR$^{-/-}$iRhom2$^{-/-}$ mice. The hepatic conversion of cholesterol into BA is a pivotal step for faecal elimination of excess cholesterol from the body and thus an essential part of lipid metabolism.[26] Hepatic BA synthesis is mainly regulated by the expression of its rate limiting enzyme CYP7A1.[27] It was reported that a high cholesterol diet induces liver inflammation and reduces hepatic CYP7A1 expression and BA synthesis, which contributes to hyperlipidaemia.[43] We corroborated that WD feeding impaired BA synthesis, as evidenced by lower hepatic BA concentration, decreased mRNA levels of CYP7A1 and its transcriptional activators HNF-4α and LRH-1 in LDLR$^{-/-}$ mice after 8 weeks of WD. In contrast, in 8 weeks WD-fed LDLR$^{-/-}$iRhom2$^{-/-}$ mice, the non-decreased hepatic BA levels indicate that iRhom2 deficiency prevents diet-induced suppression of BA synthesis. The significantly higher levels of HNF-4α mRNA and less pronounced diet-induced down-regulation of hepatic CYP7A1 and LRH-1 mRNA levels in LDLR$^{-/-}$iRhom2$^{-/-}$ mice support this assumption. HNF-4α has been identified as a critical link for TNF-α mediated repression of hepatic BA synthesis.[42] TNF-α reduces CYP7A1 expression by obstructing the transactivation activity of HNF-4α.[44] Additionally, a direct effect of TNF-α on diminishing hepatic HNF-4α mRNA and protein levels has been reported.[45]

The primary local sources of TNF-α in the liver are activated tissue-resident macrophages (Kupffer cells) and accumulation of oxidized LDL has been identified as a trigger of Kupffer cell activation in LDLR$^{-/-}$ mice.[46] Activated Kupffer cells promote infiltration of circulating CD11b+/Ly6C^{high} monocytes and trigger liver inflammation.[47] We observed that deficiency of iRhom2 did not reduce WD-induced infiltration of CD11b-positive immune cells to livers of LDLR$^{-/-}$ mice. In WD-fed LDLR$^{-/-}$iRhom2$^{-/-}$ mice, the amount of hepatic immune cells was even higher compared to WD-fed LDLR$^{-/-}$ mice, without affecting the grade of steatohepatitis. Since levels of the chemokine CCL2, known to attract Ly6C^{high} monocytes, are similar between both genotypes, we assume that this difference in hepatic immune cell content could be a consequence of the increased proportion of circulating Ly6C^{high} monocytes in iRhom2-deficient mice. Thus, the maintenance of BA synthesis and the resulting reduced hepatic lipid accumulation cannot be attributed to a reduced immune cell infiltration. This led us assume that the inability of iRhom2-deficient circulating and liver-resident immune cells to release soluble TNF-α prevents suppression of BA synthesis in the liver of WD-fed LDLR$^{-/-}$iRhom2$^{-/-}$ mice. Results from a previous study revealed a causal relationship between iRhom2/TNF-α in liver-resident macrophages and the induction of hepatic inflammation and dyslipidaemia in mice after exposure to particulate matter smaller than 2.5 μm.[48] Similarly, our observations indicate that the development of high-fat diet-induced dyslipidaemia in LDLR$^{-/-}$ mice is partially dependent on iRhom2/ADAM17 in liver-resident macrophages. As underlying mechanism, we propose a repressive effect of soluble TNF-α, cleaved from liver-resident macrophages by iRhom2-activated ADAM17, on hepatic BA synthesis via transcriptional down-regulation of HNF-4α and CYP7A1. The observed similar levels of cholesterol and TNF-α between both genotypes at 20 weeks of WD indicate that these processes are transient, which may explain the differential effects of iRhom2 deficiency observed on early and advanced atherosclerosis. Following initiation of lesion formation, atherosclerotic plaques in mice grow in a linear fashion, with a progression rate depending on the grade of hypercholesteremia.[49] The finding that iRhom2 deficiency did not influence plaque burden of advanced stages indicates that atherogenic processes mediated by iRhom2 at early atherosclerosis are absent or play a negligible role in the progression of atherosclerosis. This demonstrates that the WD-induced inflammatory immune response, which led to an increased systemic inflammation at early atherosclerosis, has changed over time and partially subsided after 20 weeks of WD. Taken together, iRhom2/ADAM17 mediated ectodomain shedding seems to enhance systemic inflammatory responses initiated by the onset of WD-feeding and accelerate early atherosclerotic plaque formation in LDLR$^{-/-}$ mice.

4.1 Limitations

Besides TNF-α, ADAM17 is involved in the cleavage of various signalling molecules.[19] We cannot exclude the contribution of other iRhom2-modulated substrates, such as amphiregulin,[12] which was recently identified as a regulator of BA synthesis by controlling CYP7A1 mRNA expression,[50] to the observed phenotype in LDLR$^{-/-}$iRhom2$^{-/-}$ mice. Moreover, we cannot rule out the possibility that modulated BA signalling contributes to the attenuation of atherosclerosis in our experiment.[51] It was reported that transgenic mice overexpressing CYP7A1 are resistant to high fat diet-induced obesity, but only in combination with an increased BA pool.[52] Our observation of reduced weight gain in iRhom2-deficient mice in the first week of WD could therefore be an indication of a change in BA signalling. Similarly, the attenuation of the diet-induced increase of triglycerides in LDLR$^{-/-}$iRhom2$^{-/-}$ mice could be explained by bile acid signalling, especially considering the observed maintenance of SHP expression.[30] We have to point out that our conclusions regarding CYP7A1, HNF-4α, and LRH-1 are based on observations at the mRNA level without supporting data at the protein level. However, it was shown that in particular the rate limiting enzyme, CYP7A1, is regulated at the mRNA level and that hepatic mRNA, protein levels and activity parallel.[27,41,45,53]

iRhom2 has emerged as a potential new target for the treatment of inflammatory diseases[15] and the present study identified the iRhom2/ADAM17 signalling axis as a critical link between inflammation, lipid metabolism and early atherogenesis. The lack of an effect of iRhom2 deficiency on advanced stage atherosclerosis in our model does not exclude potential benefits of iRhom2 inhibition on atherosclerosis in the presence of enhanced inflammation, as observed for example with diabetes mellitus or rheumatoid arthritis. The development of selective iRhom2 inhibitors represents a desirable objective to further evaluate the impact of iRhom2 on atherosclerosis.

Supplementary material

Supplementary material is available at *Cardiovascular Research* online.

Authors'contributions

C.H.: designing research studies, conducting experiments, acquiring data, analysing data, and writing the manuscript. B.H. and A.L.: designing research studies, analysing data, and writing the manuscript. A.B., J.G., N.R., A.W., and J.H.S.: conducting experiments, acquiring, and analysing data. E.A.F., V.S., and K.S.: critical revision of the manuscript.

Conflict of interest: none declared.

Funding

This work was supported by a grant of the German Research Foundation (Deutsche Forschungsgemeinschaft) (HE 6092/2-1). C.H. received a visiting scientist grant from the German Centre for Cardiovascular Research (DZHK). A.B. received a doctoral scholarship from the German Centre for Cardiovascular Research (DZHK). B.H. was a participant in the Charité Clinical Scientist Program funded by the Charité-Universitätsmedizin Berlin and the Berlin Institute of Health (BIH). E.A.F. received grants from the National Institutes of Health (HL 084312 and HL@127930).

Data Availability

The data underlying this article will be shared on reasonable request to the corresponding author.

References

1. Tuñón J, Bäck M, Badimón L, Bochaton-Piallat M-L, Cariou B, Daemen MJ, Egido J, Evans PC, Francis SE, Ketelhuth DFJ, Lutgens E, Matter CM, Monaco C, Steffens S, Stroes E, Vindis C, Weber C, Hoefer IE. Interplay between hypercholesterolaemia and inflammation in atherosclerosis: translating experimental targets into clinical practice. *Eur J Prev Cardiolog* 2018;**25**:948–955.
2. Tousoulis D, Oikonomou E, Economou EK, Crea F, Kaski JC. Inflammatory cytokines in atherosclerosis: current therapeutic approaches. *Eur Heart J* 2016;**37**:1723–1732.
3. Kleemann R, Zadelaar S, Kooistra T. Cytokines and atherosclerosis: a comprehensive review of studies in mice. *Cardiovasc Res* 2008;**79**:360–376.
4. BraNén L, Hovgaard L, Nitulescu M, Bengtsson E, Nilsson J, Jovinge S.Inhibition of tumor necrosis factor-αreduces atherosclerosis in apolipoprotein E knockout mice. *Arterioscler Thromb Vasc Biol* 2004;**24**:2137–2142.
5. Boesten LSM, Zadelaar ASM, van Nieuwkoop A, Gijbels MJJ, de Winther MPJ, Havekes LM, van Vlijmen BJM. Tumor necrosis factor-alpha promotes atherosclerotic lesion progression in APOE3-Leiden transgenic mice. *Cardiovasc Res* 2005;**66**:179–185.
6. Canault M, Peiretti F, Mueller C, Kopp F, Morange P, Rihs S, Portugal H, Juhan-Vague I, Nalbone G. Exclusive expression of transmembrane TNF-alpha in mice reduces the inflammatory response in early lipid lesions of aortic sinus. *Atherosclerosis* 2004;**172**:211–218.
7. Canault M, Peiretti F, Poggi M, Mueller C, Kopp F, Bonardo B, Bastelica D, Nicolay A, Alessi M-C, Nalbone G. Progression of atherosclerosis in ApoE-deficient mice that express distinct molecular forms of TNF-alpha. *J Pathol* 2008;**214**:574–583.
8. Black R, Rauch C, Kozlosky CJ, Peschon JJ, Slack JL, Wolfson MF, Castner BJ, Stocking KL, Reddy P, Srinivasan S, Nelson N, Boiani N, Schooley KA, Peschon JJ, Reddy P, Castner BJ, Kozlosky CJ, Cerretti DP, Srinivasan S, Stocking KL, Rauch CT, Johnson RS, March CJ, Gerhart M, Black RA, Fitzner JN, Nelson N, Wolfson MF, Paxton RJ, Davis R, Slack JL, Boiani N. A metalloproteinase disintegrin that releases tumour-necrosis factor-alpha from cells. *Nature* 1997;**385**:729–733.
9. Adrain C, Zettl M, Christova Y, Taylor N, Freeman M. Tumor necrosis factor signaling requires iRhom2 to promote trafficking and activation of TACE. SOM. *Science* 2012;**335**:225–228.
10. Siggs OM, Xiao N, Wang Y, Shi H, Tomisato W, Li X, Xia Y, Beutler B. iRhom2 is required for the secretion of mouse TNFα. *Blood* 2012;**119**:5769–5771.
11. Issuree P. A, Maretzky T, McIlwain DR, Monette S, Qing X, Lang P. A, Swendeman SL, Park-Min KH, Binder N, Kalliolias GD, Yarilina A, Horiuchi K, Ivashkiv LB, Mak TW, Salmon JE, Blobel CP. iRHOM2 is a critical pathogenic mediator of infammatory arthritis. *J Clin Invest* 2013;**123**:928–932.
12. MaretzkyT, McIlwainDR, IssureePDA, LiX, MalapeiraJ, AminS, LangPA, MakTW, BlobelCP. Blobel CP. iRhom2 controls the substrate selectivity of stimulated ADAM17-dependent ectodomain shedding. *Proc Natl Acad Sci U S A* 2013;**110**:11433–11438.
13. Franzke C-W, Cobzaru C, Triantafyllopoulou A, Löffek S, Horiuchi K, Threadgill DW, Kurz T, van Rooijen N, Bruckner-Tuderman L, Blobel CP. Epidermal ADAM17 maintains the skin barrier by regulating EGFR ligand–dependent terminal keratinocyte differentiation. *J Exp Med* 2012;**209**:1105–1119.
14. BlaydonDC, BiancheriP, DiW-L, PlagnolV, CabralRM, BrookeMA, van HeelDA, RuschendorfF, ToynbeeM, WalneA, O'TooleEA, MartinJE, LindleyK, VulliamyT, AbramsDJ, MacDonaldTT, HarperJI, KelsellDP. Inflammatory skin and bowel disease linked to ADAM17 deletion. *N Engl J Med* 2011;**365**:1502–1508.
15. Geesala R, Issuree PD, Maretzky T. Novel functions of inactive rhomboid proteins in immunity and disease. *J Leukoc Biol* 2019;**106**:823–835.
16. Van Hauwermeiren F, Vandenbroucke RE, Libert C. Treatment of TNF mediated diseases by selective inhibition of soluble TNF or TNFR1. *Cytokine Growth Factor Rev* 2011;**22**:311–319.
17. Qing X, Chinenov Y, Redecha P, Madaio M, Roelofs JJTH, Farber G, Issuree PD, Donlin L, McIlwain DR, Mak TW, Blobel CP, Salmon JE. iRhom2 promotes lupus nephritis through TNF-α and EGFR signaling. *J Clin Invest* 2018;**128**:1397–1412.
18. Chemaly M, Mcgilligan V, Gibson M, Clauss M, Watterson S, Alexander HD, John A, Peace A. Role of tumour necrosis factor alpha converting enzyme (TACE/ADAM17) and associated proteins in coronary artery. *Arch Cardiovasc Dis* 2017;**110**:700–711.
19. Scheller J, Chalaris A, Garbers C, Rose-John S. ADAM17: a molecular switch to control inflammation and tissue regeneration. *Trends Immunol* 2011;**32**:380–387.
20. Chaohui C, Wei H, Hongfeng W, Yueliang Z, Xiaoqin P, Pingli Z, Zhibing A. iRhom2 promotes atherosclerosis through macrophage inflammation and induction of oxidative stress. *Biochem Biophys Res Commun* 2018;**503**:1897–1904.
21. Kleiner DE, Brunt EM, Van Natta M, Behling C, Contos MJ, Cummings OW, Ferrell LD, Liu Y-C, Torbenson MS, Unalp-Arida A, Yeh M, McCullough AJ, Sanyal AJ, Nonalcoholic Steatohepatitis Clinical Research Network. Design and validation of a histological scoring system for nonalcoholic fatty liver disease. *Hepatology* 2005;**41**:1313–1321.
22. Yeh MM, Brunt EM. Pathological features of fatty liver disease. *Gastroenterology* 2014;**147**:754–764.
23. MacDonald KPA, Palmer JS, Cronau S, Seppanen E, Olver S, Raffelt NC, Kuns R, Pettit AR, Clouston A, Wainwright B, Branstetter D, Smith J, Paxton RJ, Cerretti DP, Bonham L, Hill GR, Hume DA. An antibody against the colony-stimulating factor 1 receptor depletes the resident subset of monocytes and tissue- and tumor-associated macrophages but does not inhibit inflammation. *Blood* 2010;**116**:3955–3963.
24. Horiuchi K, Miyamoto T, Takaishi H, Hakozaki A, Kosaki N, Miyauchi Y, Furukawa M, Takito J, Kaneko H, Matsuzaki K, Morioka H, Blobel CP, Toyama Y. Cell surface colony-stimulating factor 1 can be cleaved by TNF-converting enzyme or endocytosed in a clathrin-dependent manner. *J Immunol* 2007;**179**:6715–6724.
25. Rovida E, Paccagnini A, Del Rosso M, Peschon J, Dello Sbarba P. TNF-α-converting enzyme cleaves the macrophage colony-stimulating factor receptor in macrophages undergoing activation. *J Immunol* 2001;**166**:1583–1589.
26. Temel RE, Brown JM. Biliary and nonbiliary contributions to reverse cholesterol transport. *Curr Opin Lipidol* 2012;**23**:85–90.
27. Chiang JYL. Bile acids: regulation of synthesis. *J Lipid Res* 2009;**50**:1955–1966.
28. Kir S, Zhang Y, Gerard RD, Kliewer SA, Mangelsdorf DJ. Nuclear receptors HNF4α and LRH-1 cooperate in regulating Cyp7a1 in vivo. *J Biol Chem* 2012;**287**:41334–41341.
29. Davis RA, Miyake JH, Hui TY, Spann NJ. Regulating of cholesterol-7alpha-hydroxylase: BAREly missing a SHP. *J Lipid Res* 2002;**43**:533–543.
30. Watanabe M, Houten SM, Wang L, Moschetta A, Mangelsdorf DJ, Heyman RA, Moore DD, Auwerx J. Bile acids lower triglyceride levels via a pathway involving FXR, SHP, and SREBP-1c. *J Clin Invest* 2004;**113**:1408–1418.
31. Crestani M, De Fabiani E, Caruso D, Mitro N, Gilardi F, Vigil Chacon AB, Patelli R, Godio C, Galli G. LXR (liver X receptor) and HNF-4 (hepatocyte nuclear factor-4): key regulators in reverse cholesterol transport. *Biochem Soc Trans* 2004;**32**:92–96.
32. Lloyd CM, Phillips ARJ, Cooper GJS, Dunbar PR. Three-colour fluorescence immunohistochemistry reveals the diversity of cells staining for macrophage markers in murine spleen and liver. *J Immunol Methods* 2008;**334**:70–81.
33. Romee R, Foley B, Lenvik T, Wang Y, Zhang B, Ankarlo D, Luo X, Cooley S, Verneris M, Walcheck B, Miller J. NK cell CD16 surface expression and function is regulated by a disintegrin and metalloprotease-17 (ADAM17). *Blood* 2013;**121**:3599–3608.
34. Yona S, Kim K-W, Wolf Y, Mildner A, Varol D, Breker M, Strauss-Ayali D, Viukov S, Guilliams M, Misharin A, Hume DA, Perlman H, Malissen B, Zelzer E, Jung S. Fate mapping reveals origins and dynamics of monocytes and tissue macrophages under homeostasis. *Immunity* 2013;**38**:79–91.
35. Qing X, D. Rogers L, Mortha A, Lavin Y, Redecha P, Issuree PD, Maretzky T, Merad M, R. McIlwain D, Mak TW, Overall CM, Blobel CP, Salmon JE. iRhom2 regulates

CSF1R cell surface expression and non-steady state myelopoiesis in mice. *Eur J Immunol* 2016;**46**:2737–2748.
36. Tang J, Frey JM, Wilson CL, Moncada-Pazos A, Levet C, Freeman M, Rosenfeld ME, Stanley ER, Raines EW, Bornfeldt KE. Neutrophil and macrophage cell surface colony-stimulating factor 1 shed by ADAM17 drives mouse macrophage proliferation in acute and chronic inflammation. *Mol Cell Biol* 2018;**38**:1–19.
37. Dai X-M, Zong X-H, Sylvestre V, Stanley ER. Incomplete restoration of colony-stimulating factor 1 (CSF-1) function in CSF-1-deficient Csf1op/Csf1op mice by transgenic expression of cell surface CSF-1. *Blood* 2004;**103**:1114–1123.
38. McLaren JE, Ramji DP. Interferon gamma: a master regulator of atherosclerosis. *Cytokine Growth Factor Rev* 2009;**20**:125–135.
39. Hilgendorf I, Swirski FK, Robbins CS. Monocyte fate in atherosclerosis. *Arterioscler Thromb Vasc Biol* 2015;**35**:272–279.
40. Chen Y, Chen Y, Zhao L, Chen Y, Mei M, Li Q, Huang A, Varghese Z, Moorhead JF, Ruan XZ. Inflammatory stress exacerbates hepatic cholesterol accumulation via disrupting cellular cholesterol export. *J Gastroenterol Hepatol* 2012;**27**:974–984.
41. Miyake JH, Wang SL, Davis RA. Bile acid induction of cytokine expression by macrophages correlates with repression of hepatic cholesterol 7α-hydroxylase. *J Biol Chem* 2000;**275**:21805–21808.
42. De Fabiani E, Mitro N, Anzulovich AC, Pinelli A, Galli G, Crestani M. The negative effects of bile acids and tumor necrosis factor-α on the transcription of cholesterol 7α-hydroxylase gene (CYP7A1) converge to hepatic nuclear factor-4: a novel mechanism of feedback regulation of bile acid synthesis mediated by nuclear recep. *J Biol Chem* 2001;**276**:30708–30716.
43. Henkel AS, Anderson KA, Dewey AM, Kavesh MH, Green RM. A chronic high-cholesterol diet paradoxically suppresses hepatic CYP7A1 expression in FVB/NJ mice. *J Lipid Res* 2011;**52**:289–298.
44. Babeu JP, Boudreau F. Hepatocyte nuclear factor 4-alpha involvement in liver and intestinal inflammatory networks.*World J Gastroenterol* 2014;**20**:22–30.
45. SimóR, Barbosa-Desongles A, Lecube A, Hernandez C, Selva DM. Potential role of tumor necrosis factor-α in downregulating sex hormone-binding globulin. *Diabetes* 2012;**61**:372–382.
46. Bieghs V, Walenbergh SMA, Hendrikx T, van Gorp PJ, Verheyen F, Olde Damink SW, Masclee AA, Koek GH, Hofker MH, Binder CJ, Shiri-Sverdlov R. Trapping of oxidized LDL in lysosomes of Kupffer cells is a trigger for hepatic inflammation. *Liver Int* 2013;**33**:1056–1061.
47. Tosello-Trampont A-C, Landes SG, Nguyen V, Novobrantseva TI, Hahn YS. Kuppfer cells trigger nonalcoholic steatohepatitis development in diet-induced mouse model through tumor necrosis factor-αproduction. *J Biol Chem* 2012;**287**:40161–40172.
48. Ge C-X, Qin Y-T, Lou D-S, Li Q, Li Y-Y, Wang Z-M, Yang W-W, Wang M, Liu N, Wang Z, Zhang P-X, Tu Y-Y, Tan J, Xu M-X. iRhom2 deficiency relieves TNF-α associated hepatic dyslipidemia in long-term PM2.5-exposed mice. *Biochem Biophys Res Commun* 2017;**493**:1402–1409.
49. Kowala MC, Recce R, Beyer S, Gu C, Valentine M. Characterization of atherosclerosis in LDL receptor knockout mice: macrophage accumulation correlates with rapid and sustained expression of aortic MCP-1/JE. *Atherosclerosis* 2000;**149**:323–330.
50. Santamaría E, Rodríguez-Ortigosa CM, Uriarte I, Latasa MU, Urtasun R, Alvarez-Sola G, Bárcena-Varela M, Colyn L, Arcelus S, Jiménez M, Deutschmann K, Peleteiro-Vigil A, Gómez-Cambronero J, Milkiewicz M, Milkiewicz P, Sangro B, Keitel V, Monte MJ, Marin JJG, Fernández-Barrena MG, Ávila MA, Berasain C. The epidermal growth factor receptor ligand amphiregulin protects from cholestatic liver injury and regulates bile acids synthesis. *Hepatology* 2019;**69**:1632–1647
51. Pols TWH, Nomura M, Harach T, Lo Sasso G, Oosterveer MH, Thomas C, Rizzo G, Gioiello A, Adorini L, Pellicciari R, Auwerx J, Schoonjans K. TGR5 activation inhibits atherosclerosis by reducing macrophage inflammation and lipid loading. *Cell Metab* 2011;**14**:747–757.
52. Li T, Owsley E, Matozel M, Hsu P, Novak CM, Chiang JYL. Transgenic expression of cholesterol 7α-hydroxylase in the liver prevents high-fat diet-induced obesity and insulin resistance in mice. *Hepatology* 2010;**52**:678–690.
53. Feingold KR, Spady DK, Pollock AS, Moser AH, Grunfeld C. Endotoxin, TNF, and IL-1 decrease cholesterol 7α-hydroxylase mRNA levels and activity. *J Lipid Res* 1996;**37**:223–228.

Translational Perspective

iRhom2 attenuates shedding of TNF-α selectively from immune cells and therefore has emerged as a potential new target for the treatment of inflammatory diseases. In the present study, we identified iRhom2 as a critical link between inflammation, lipid metabolism, and atherogenesis. Selective iRhom2 inhibition represents a potential treatment strategy to modify atherosclerosis, particularly in the presence of enhanced inflammation as observed with diabetes mellitus or rheumatoid arthritis.